Modeling dynamics of ECT-2/AIR-1 on the cortex

Ondrej Maxian

March 8, 2024

1 The centrosome cue

The contractility circuit is forced by a cue from the centrosomes which contain Aurora A (AIR-1), an inhibitor of ECT-2. We assume that the AIR-1 signal gets to the membrane by diffusion. Letting $a(\boldsymbol{x})$ be the concentration of AIR-1 in the embryo, we have the equation

$$\Delta a = -f \qquad \boldsymbol{x} \in \Omega \tag{1a}$$

$$\nabla a \cdot \boldsymbol{n} = 0 \quad \boldsymbol{x} \in \partial\Omega, \tag{1b}$$

where (1a) is the diffusion equation for the concentration and (1b) is a no-flux boundary condition through the boundary (here Ω represents the embryo area and $\partial\Omega$ represents the boundary). The signal $f(\boldsymbol{x})$ comes from the two centrosomes, which we model by Gaussian densities

$$f(\boldsymbol{x}) = \frac{C_0/D}{2\pi\sigma_c^2}\sum_{i=1}^{2}\exp\left(\frac{-\|\boldsymbol{x}-\boldsymbol{x}_i\|^2}{2\sigma_c^2}\right). \tag{1c}$$

Here $\boldsymbol{x}_i$ is the location of the ith centrosome (typically at some location $(x_i, 0)$), which changes depending on the embryo conditions. In addition to the centrosome location, the signal has two other parameters: C_0/D is the strength of the cue (the integral of $f(\boldsymbol{x})$ over the entire embryo cross-section, normalized by the cytoplasmic diffusion coefficient D), and σ_c is the centrosome "size" (the standard deviation of the Gaussian, which is roughly half the size of the centrosome). For cytokinesis, the centrosomes have size about 2 μm, so we set $\sigma_c = 1$ μm. The solution of (1a) is unique up to a constant; thus, when we compare profiles to each other we can only speak of concentration *differences* rather than absolute concentration.

We use a standard first-order finite element method to solve (1a). In brief, the elliptical domain of the embryo is meshed into nodes and triangles, which define a set of linear Lagrangian basis functions ψ_k that are 1 at node $\boldsymbol{x}_k$ and 0 everywhere else. Multiplying (1a) by a basis function ψ_k,

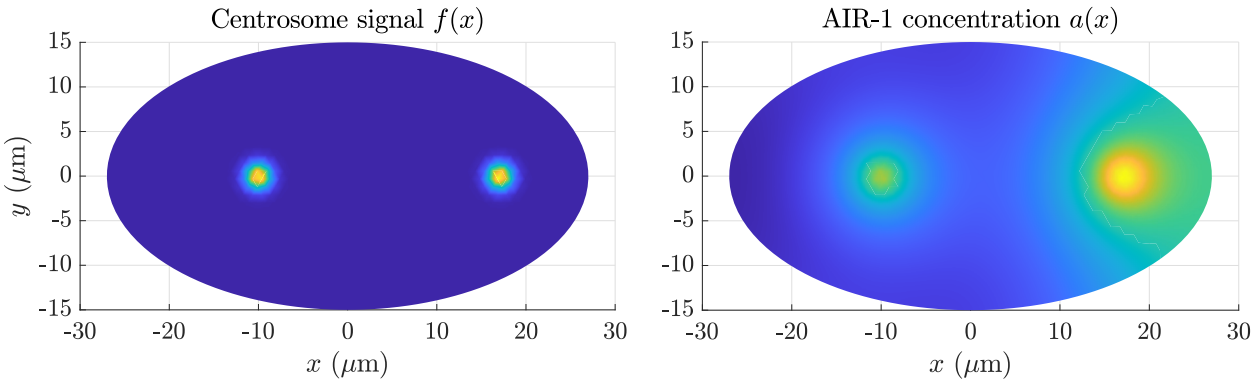

Figure 1: Solution for the diffusion equation (1) for wild-type embryos. The left panel shows the centrosome signal $f(\boldsymbol{x})$, with the anterior centrosome 17 μm away from the anterior cortex and the posterior centrosome 10 μm away from the posterior cortex. The Gaussian width $\sigma_c = 1$ (so that the centrosome diameter is roughly 2 μm). The right panel shows the solution for the concentration profile $a(\boldsymbol{x})$.

then integrating by parts using the boundary condition (1b) gives

$$\sum_j \int_\Omega (\nabla\psi_k \cdot \nabla\psi_j)\, a_j \, d\boldsymbol{x} = \sum_j \int_\Omega \psi_k \psi_j f_j \, d\boldsymbol{x}, \tag{2}$$

which can be written as the matrix equation $\boldsymbol{K}\boldsymbol{a} = \boldsymbol{M}\boldsymbol{f}$, where $\boldsymbol{M}$ is the so-called mass matrix and $\boldsymbol{K}$ the stiffness matrix for finite elements. Solving $\boldsymbol{a} = \boldsymbol{K}^\dagger \boldsymbol{M}\boldsymbol{f}$ gives the solution for the concentration.

Figure 1 shows the solution of the diffusion equation over the embryo cross-section in wild-type embryos. In this case, the anterior centrosome sits 17 μm from the anterior pole, while the posterior centrosome sits 10 μm from the posterior pole. The left panel shows the AIR-1 signal, which essentially shows the location of the two centrosomes. The right panel then shows the solution to the diffusion equation (1) in this case. As might be expected, there is substantially more AIR-1 on the anterior cortex, since the centrosome sits closer to the boundary there.

We now consider how moving the centrosomes changes the profile of AIR-1 on the boundary. We use six representative treatments from [2], which modify the positions of the centrosomes, and plot the results in Fig. 2. As an example, in dhc-1 (RNAi) embryos, the posterior centrosome sits 3 μm from the posterior pole, while the anterior centrosome sits 45 μm from the anterior pole (9 μm from the posterior pole). As a result, the AIR-1 profile is strongly peaked at the posterior, with an AIR-1 gradient about 6 times larger than the wild-type. The treatments we consider can also flatten the AIR-1 profile relative to wild-type, as in PAR-3 (RNAi) embryos, which have

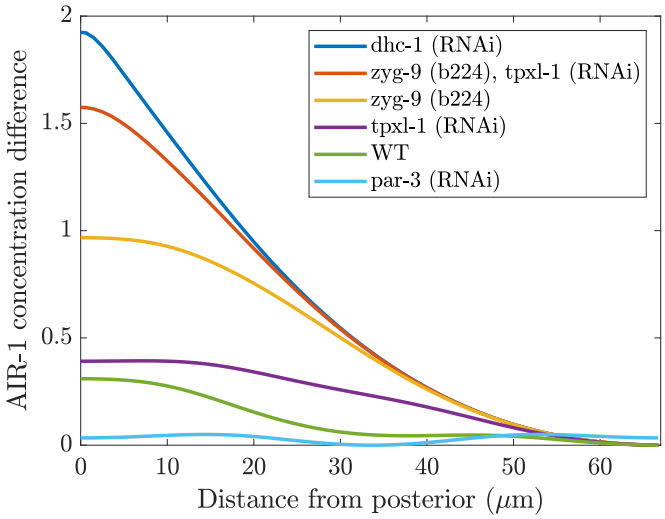

Figure 2: AIR-1 accumulation on the embryo perimeter (cortex) as predicted by the diffusion model (1). We show the AIR-1 profile as a function of distance from the posterior pole (0 is the posterior pole, 67 is the anterior pole), for embryos with six different treatments. The treatment sets the location of the centrosomes (see Fig. 5).

centrosomes sitting roughly at 15 μm from each pole. The profile of AIR-1 there is consequently roughly constant.

1.1 Adding AIR-1 inactivation

We also consider the case when there is a basal level of inactivation of AIR-1 in the cytoplasm. To model this, we modify (1a) to add an additional inactivation term

$$\Delta a - \bar{k}^{\text{off}} a = -f \qquad \boldsymbol{x} \in \Omega. \tag{3}$$

This introduces another parameter which is the inactivation rate relative to the diffusion coefficient in the cytoplasm (units μm^{-2}). Solving (3) with the finite element is very simple: the matrix equation becomes $\left(\boldsymbol{K} + \bar{k}^{\text{off}}\boldsymbol{M}\right)\boldsymbol{a} = \boldsymbol{M}\boldsymbol{f}$. An advantage of this approach is that the solution for concentration is unique (no longer an unknown constant).

Figure 3 shows the effect of the new inactivation term in the model, both in the cross-sectional profile of AIR-1, and also along the embryo perimeter from posterior to anterior. We find that $\bar{k}^{\text{off}} \leq 10^{-3}$ μm^{-2} preserves the general trend we observed previously in wild-type embryos, where the concentration is about 0.3 units higher at the posterior than the anterior. Increasing the inactivation rate leads to more of the AIR-1 being inactivated prior to reaching the posterior pole,

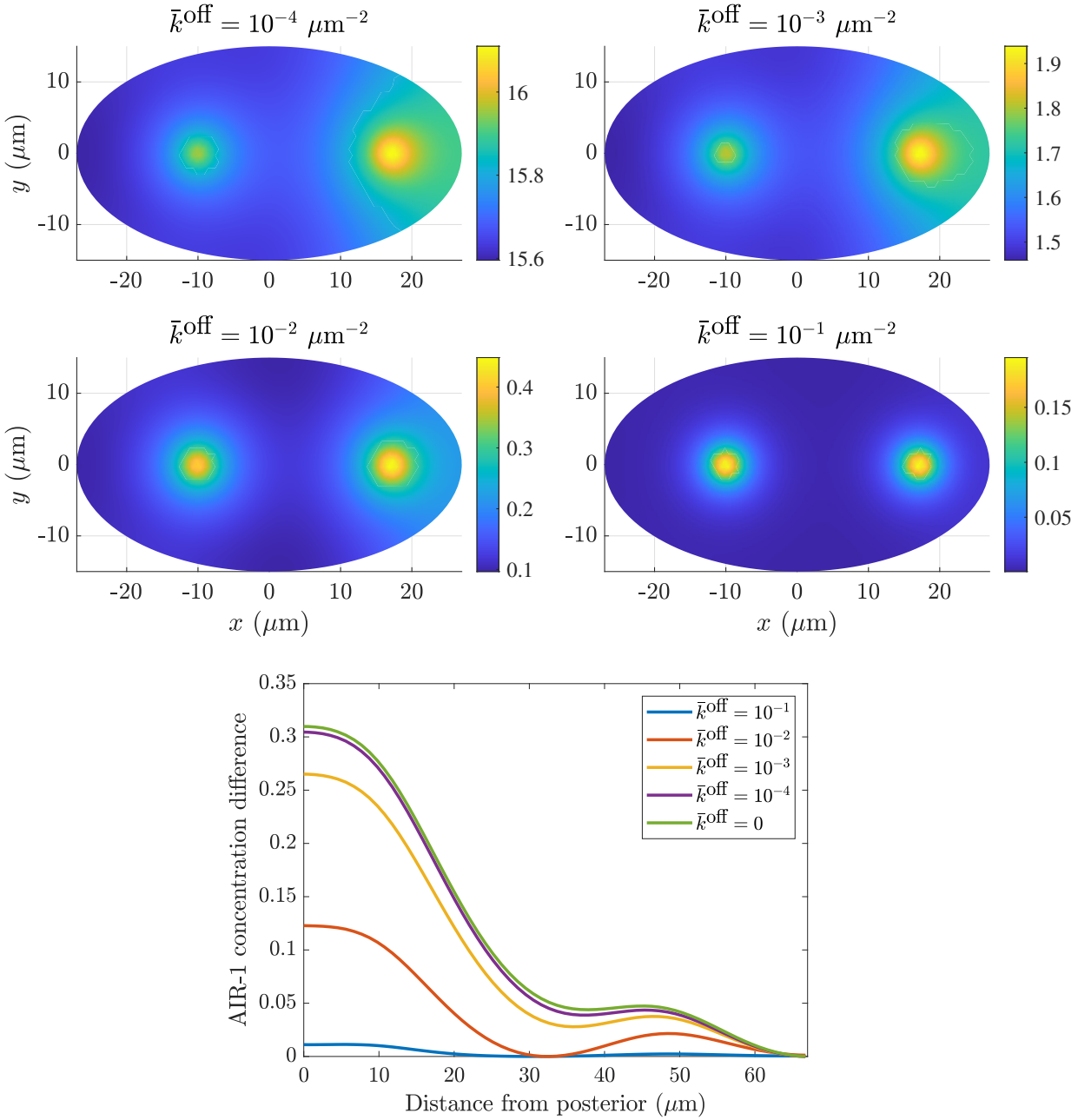

Figure 3: Profile of AIR-1 in wild-type embryo, obtained by solving (3) with different values of $\bar{k}^{\text{off}} = k^{\text{off}}/D$. The top plots show the profile along the whole embryo when changing $\bar{k}^{\text{off}}$; the bottom (summary) plot shows the change in the AIR-1 concentration (relative to the anterior pole) along the embryo perimeter.

which causes the gradient to drop (for $\bar{k}^{\text{off}} = 10^{-2}\ \mu\text{m}^{-2}$), and then vanish (for $\bar{k}^{\text{off}} = 10^{-1}\ \mu\text{m}^{-2}$).

1.2 The ECT-2 response

Let us now examine how the strength of the AIR-1 signal affects the strength of the ECT-2 concentration on the proximal cortex. To do so, let us suppose that ECT-2 locally binds and unbinds from the cortex, with AIR-1 increasing the unbinding rate. At steady state, this gives the equation

$$k_E^{\text{on}} = k_E^{\text{off}} \left(1 + K_{\text{AE}} \left(A - A_{\text{min}}\right)\right) E \rightarrow E = \frac{k_E^{\text{on}}/k_E^{\text{off}}}{1 + K_{\text{AE}} \left(A - A_{\text{min}}\right)} \tag{4}$$

where K_{AE} is the strength of AIR-1/ECT-2 inhibition, and A_{min} is the minimum level of AIR-1 across all embryo conditions. To fit the parameters in this model, we use the AIR-1 concentration data *with inactivation* (Section 1.1), so that the absolute concentrations are well defined. We set $\bar{k}^{\text{off}} = 10^{-3}\ \mu\text{m}^{-2}$, since this corresponds to a slight weakening of the diffusion (check parameters), which results in the AIR-1 profiles shown in the left panel of Fig. 4. The parameter $A_{\text{min}} = 1.1$ is set to the minimum AIR-1 concentration across all embryos, and then $k_E^{\text{on}}/k_E^{\text{off}} = 2.5$ is obtained by fitting the maximum ECT-2 accumulation from experimental data (dhc-1 (RNAi) embryos). The last parameter $K_{\text{AE}} = 1.3$ is set to match the minimum ECT-2 accumulation of 0.8 when AIR-1 is at its maximum (about 2.8 in dhc-1 (RNAi) embryos). The right panel of Fig. 4 shows the resulting ECT-2 profiles we obtain across different conditions.

Figure 5 compares the resulting output (right panel) to the experimental data (left panel). While we can generally reproduce the trends observed experimentally, the shape of our curve appears to be more of a line, while the experimental data show an S-shaped trend. Indeed, while we correctly predict the ECT-2 accumulation for the "extreme" embryos (dhc-1 (RNAi) and zyg-9 (b224)/tpxl-1(RNAi)), the intermediate embryos have A/P ECT-2 disparities which are smaller than the experimental data. For example, in wild-type embryos, the experiments show an accumulation of 1.8 on the posterior, and 1 on the anterior, while our results show an accumulation of 1.7 on the posterior and 1.4 on the anterior.

Because we chose parameters to match dhc-1 (RNAi) embryos, their values are correct by design. If, by contrast, we had chosen a larger K_{AE} to match wild-type embryos, then the model results would be reversed: the wild-type embryos would be correct by design, while the extreme embryos would have A/P ratios which are much *larger* than the experiments. It seems clear that our model is missing a mechanism whereby either:

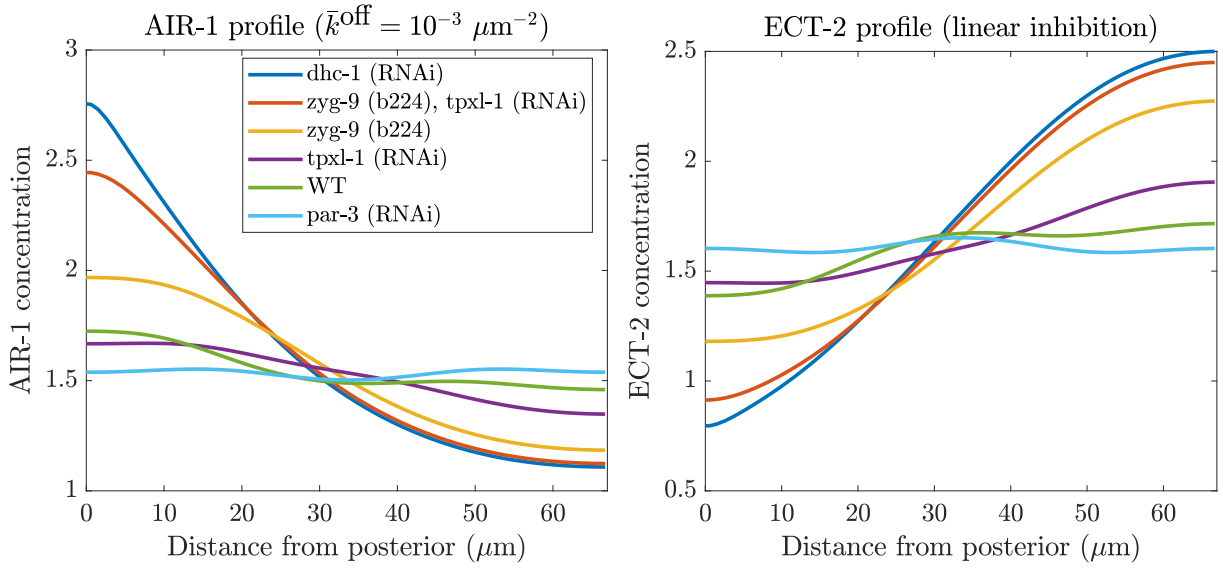

Figure 4: AIR-1 and ECT-2 profiles assuming linear inhibition model (4). The AIR-1 profiles are obtained by solving (3) with the different centrosome distances obtained from [2] and $\bar{k}^{\text{off}} = 10^{-3}$ μm^{-2}. The ECT-2 profiles are then obtained from (4), where we set $A_{\min} = 1.1$, $k_E^{\text{on}}/k_E^{\text{off}} = 2.5$, and $K_{\text{AE}} = 1.3$.

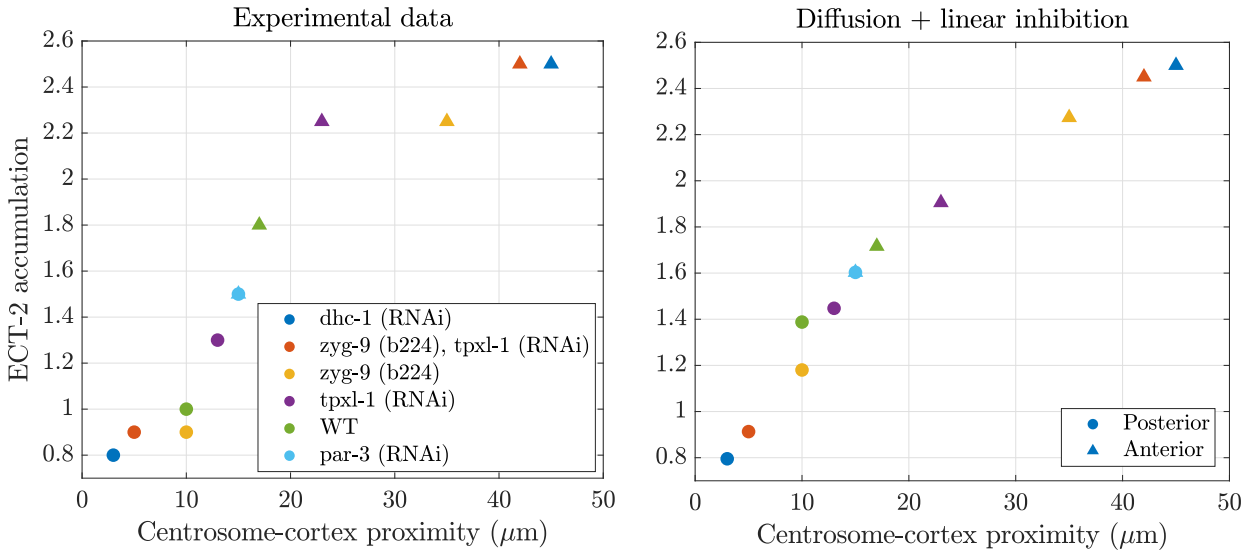

Figure 5: Comparing model results to experimental data for embryos with varying treatments (see legend at left). The left plot is a reproduction of [2, Fig. 7A], with some of the redundant embryo treatments deleted for clarity (we reduce multiple replicates to a single symbol by taking a rough average). The right plot shows the results when we consider diffusion of AIR-1 to the cortex, plus linear inhibition of the form (4) (see Fig. 4 for details).

1. Small changes in ECT-2 concentration induced by diffusion (in an intermediate range) are amplified to become larger.

2. Large changes in ECT-2 concentration induced by diffusion are damped to become smaller.

Since we have not accounted for the resulting actomyosin flows which tend to concentrate ECT-2, we speculate that the first of these options is what is missing from the model. We proceed to study it next.

1.3 Flows by myosin

We now explore the possibility that flows due to myosin could propagate smaller ECT-2 asymmetries into larger ones. To do this, we consider the basic model that ECT-2 (through activating ρ) activates myosin at the cortex. To minimze the number of parameters, we consider a simplified version of the diagram in Fig. 8 where there are only two species: ECT-2 (E) and myosin (M). In a system of units where length is in units of the embryo perimeter L, and time is in units of the bound myosin lifetime $1/k_M^{\text{off}}$, the general equations governing this system can be written as

$$\partial_t E + \sigma_0 \partial_x (vE) = D_E \partial_x^2 E + K_E^{\text{on}} E_c - K_E^{\text{off}} \left(1 + K_{\text{AE}} \left(A - A_{\min}\right)\right) E \tag{5a}$$

$$\partial_t M + \sigma_0 \partial_x (vM) = D_M \partial_x^2 M + K_M^{\text{on}} \left(1 + K_{\text{EM}} E\right) M_c - M \tag{5b}$$

$$v = \ell^2 \partial_x^2 v + \ell \partial_x \left(\frac{M}{M_c + M}\right) \tag{5c}$$

$$E_c = 1 - \int_0^1 E(x)\, dx \qquad M_c = 1 - \int_0^1 M(x)\, dx \tag{5d}$$

where $K_E^{\text{off}} = k_E^{\text{off}}/k_M^{\text{off}}$ expresses the lifetime of ECT-2 relative to that of myosin. The first two equations are relatively straightforward; we have binding of ECT-2 to the membrane, with AIR-1 inhibiting ECT-2 (by promoting unbinding) according to the relationship (4) and ECT-2 linearly promoting myosin. To choose unknown parameters, we first fix K_E^{off} according to experimental data, then choose K_E^{on} so that 10% of the total ECT-2 is bound to the cortex. We then set $K_{\text{EM}} = 10$, so that (accounting for $E \approx 0.1$), the term $K_{\text{EM}} E \approx 1$, meaning that the basal rate of myosin binding is equal to that promoted by ECT-2.

In the velocity equation (6f), the variable ℓ is the hydrodynamic lengthscale (approximately 10 μm [3], and the expression $M/(M + M_c)$ gives the tension myosin exerts. We use this form so that myosin can build up until $M \approx 2M_c$, after which tension becomes roughly constant. In doing this, we artificially prevent the focusing of myosin into infinitely thin peaks. We set $K_M^{\text{on}} = 0.2$ so that

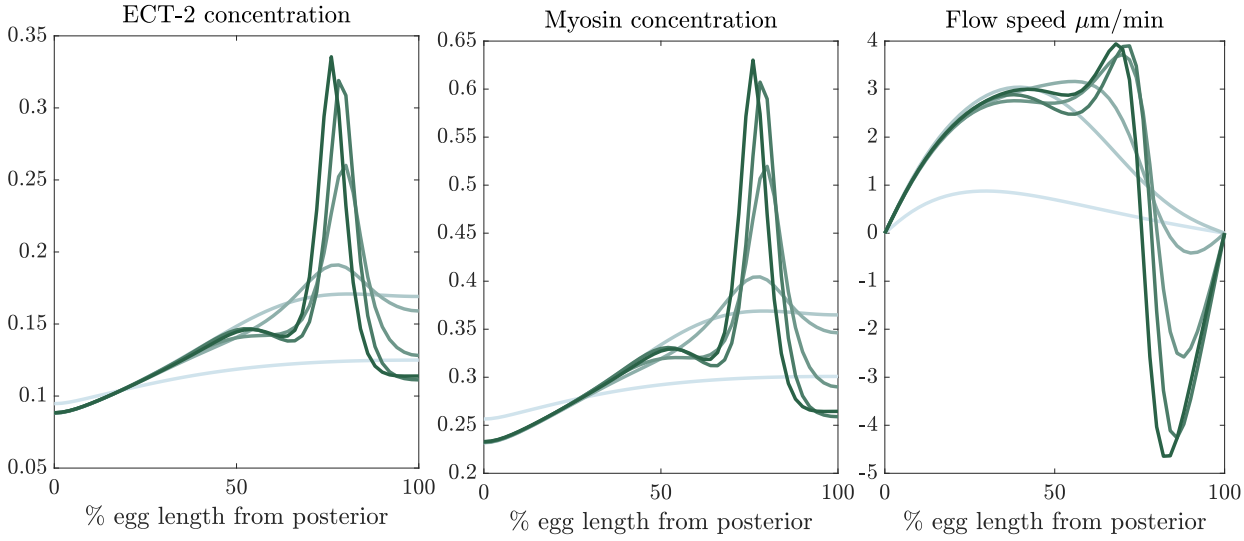

(a) dhc-1 (RNAi)

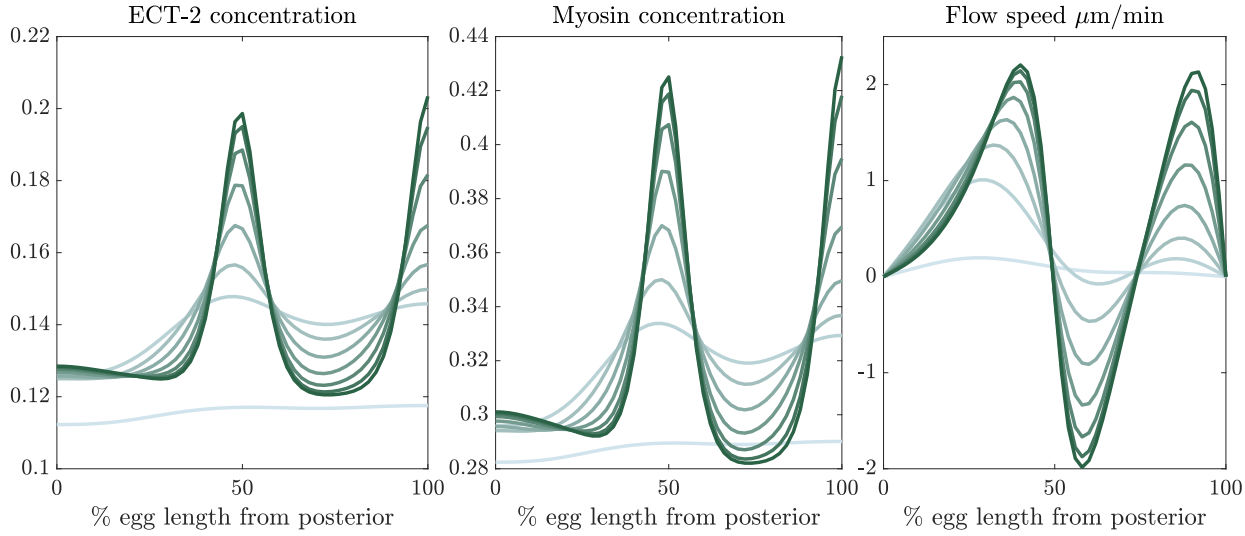

(b) Wild type

Figure 6: Trajectory with flows.

there is typically about 30% bound myosin, then set $M_c = 0.25$ so that exceeding $M \approx 0.5$ leads to a plateau in stress. Finally, the coefficient σ_0 (which we will vary) expresses the speed of the flow; increasing σ_0 increases the flow speed for a given tension profile.

In [2], FRAP measurements showed the lifetime of a typical ECT-2 molecule to be on the order of a few seconds. Considering this, we first take $k_E^{\text{off}} = 0.2\ \text{s}^{-1}$, so that the lifetime is 5 seconds. We then vary the coefficient σ_0 to change the speed of flow. As show in Fig. 6(a), there is not substantial transport of ECT-2 molecules (and a change in the ECT-2 profile) until the flow speed reaches some 12 μm/min, which is much faster than the typically observed flow speeds. We fare better when we increase the residence time of ECT-2; in Fig. 6(b) we show that a 50 second residence time ($k_E^{\text{off}} = 0.02$/s) leads to a strong change in the ECT-2 profile at more realistic (at most 4 μm/min) flow speeds. Still, there are no experiments which establish that ECT-2 could be bound to the cortex this long.

In addition, there is a second major problem relating to this circuit. We saw previously that, when our diffusion data is fit to the embryos with the maximum ECT-2 asymmetries, the wild-type embryos have a weak asymmetry. We then considered that flow could amplify this asymmetry. But flow depends on ECT-2 asymmetries, so embryos with larger asymmetries will have *larger* amplification by flow. In other words, this flow model will affect embryos with larger ECT-2 asymmetries more than the embryos in the middle, which is the exact opposite of our intention.

There is another major problem with this model: it relies on an instability in the myosin dynamics to obtain flows. In other words, a small perturbation in myosin leads to growth of an instability which concentrates myosin into peaks. In this model, the peaks tend to be highly dynamic and shift around, growing and shrinking in time. This is not what is observed in live embryos. Indeed, studies have shown that the system is *not* spontaneously unstable, but relies on cues which reorganize the PAR protein network to stably maintain asymmetries [1].

2 The biochemical response circuit

The following is old We now consider how the underlying biochemical system might respond to changes in the ECT-2 signal at the cortex.We consider four species: ECT-2 (E), inactive Rho (P), active Rho (ρ), and actomyosin (M), with interactions shown in Fig. 8. The main question we need to answer is the functional form by which inactive Rho and active Rho are exchanged/converted amongst each other. Based on the analysis of [5], we assume the reaction to be auto-catalytic (the

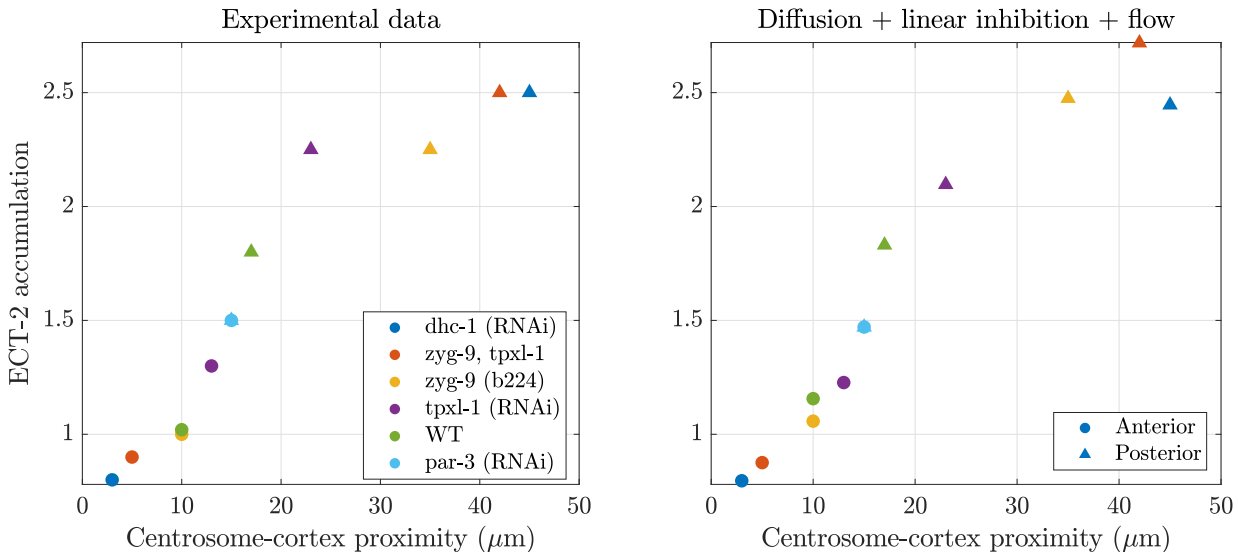

Figure 7

forward rate is proportional to active ρ). Based on the data that ECT-2 has a roughly 2:1 A/P ratio, while ρ has a roughly 10:1 ratio, we assume nonlinearity in E as well. Finally, we assume that actomyosin M converts active Rho to inactive Rho via RhoGAP (which colocalizes with actin) [5]. Our total reaction term is therefore,

$$R(P,\rho,E,M) = K_{\mathrm{EP}} E^2 \left(\frac{\rho}{G_{\mathrm{PP}} + \rho} \right) P - K_{\mathrm{MP}} M \rho, \tag{6a}$$

which leaves three unknown constants: K_{EP}, K_{MP}, and G_{PP}.

Once we formulate the reaction term converting inactive Rho to active Rho, it is straightforward to formulate the rest of the dynamics. As in [4], we assume that inactive Rho binds from the cytoplasm onto the membrane, where it is converted to active Rho using (6a). Once active, ρ produces myosin. In a system of units where length is in units of the embryo perimeter L, and time is in units of the bound myosin lifetime $1/k_M^{\mathrm{off}}$, the general equations governing the circuit can

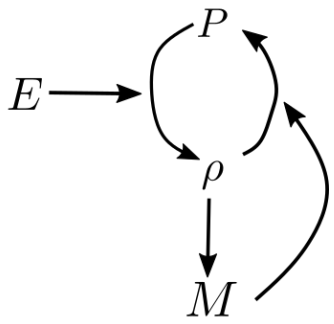

Figure 8: The circuit we consider in this report.

consequently be written as

$$\partial_t E + \sigma_0 \partial_x (vE) = D_E \partial_x^2 E + K_E^{\text{on}} E_c - K_E^{\text{off}} (1 + K_{\text{AE}} A) E \tag{6b}$$

$$\partial_t P + \sigma_0 \partial_x (vP) = D_P \partial_x^2 P + K_P^{\text{on}} P_c - K_E^{\text{off}} P - R(P, \rho, E, M) \tag{6c}$$

$$\partial_t \rho + \sigma_0 \partial_x (v\rho) = D_\rho \partial_x^2 \rho + R(P, \rho, E, M) \tag{6d}$$

$$\partial_t M + \sigma_0 \partial_x (vM) = D_M \partial_x^2 M + K_M^{\text{on}} \left(1 + K_{\text{PM}} \frac{\rho}{G_{\text{PM}} + \rho}\right) M_c - M \tag{6e}$$

$$v = \ell^2 \partial_x^2 v + \ell \partial_x M \tag{6f}$$

$$E_c = 1 - \int_0^1 E(x)\, dx \qquad P_c = 1 - \int_0^1 \left(P(x) + \rho(x)\right)\, dx \qquad M_c = 1 - \int_0^1 M(x)\, dx \tag{6g}$$

In the velocity equation (6f), the lengthscale ℓ is a hydrodynamic lengthscale (roughly 10 μm), normalized in this unit system by the embryo perimeter [6]. The constant $\sigma_0 \approx 0.026$ is the scale of the active stres induced by myosin, and has been determined elsewhere, along with the form of the stress itself $\sigma_a = M$.

Discounting the off and on rates, which can be determined directly and from the percentage of protein that is bound at steady state, respectively, there are a total of six unknown constants: K_{EP}, K_{MP}, G_{PP} (in the Rho reaction), and K_{AE}, K_{PM}, and G_{PM} (in the other reactions). Figure **??** tells us that $K_{\text{AE}} \approx 1$. To set the parameters K_{EP}, K_{MP}, and K_{PM}, we look for a regime where roughly 10% of bound Rho is active, and the asymmetry in active Rho is about 10:1. We do this by first specifying G_{PM} and G_{PP}. Far below these constants, the ρ signal is linear, while above them it saturates. We want to operate in the linear regime, and since we expect about 10% of the Rho to be bound to the membrane, we take $G_{\text{PM}} = G_{\text{PP}} = 0.2$. The other parameters are set so that we have a roughly 10:1 asymmetry in myosin and active Rho. The steady state results are shown in Fig. 9.

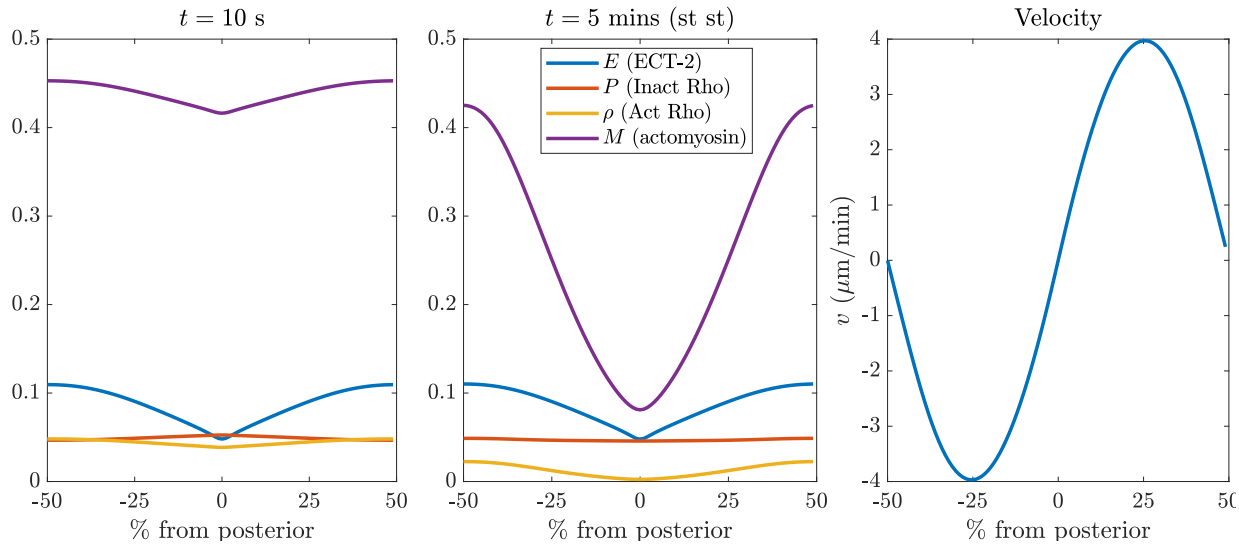

Figure 9: How the AIR-1 signal and ECT-2 profile set the downstream concentrations. Left plot: initially, ECT-2 assumes its asymmetric profile. Middle plot: this sets up a steady state with asymmetric myosin and active Rho. Right plot: velocity at steady state in μm/min.

References

[1] Peter Gross, K Vijay Kumar, Nathan W Goehring, Justin S Bois, Carsten Hoege, Frank Jülicher, and Stephan W Grill. Guiding self-organized pattern formation in cell polarity establishment. *Nature physics*, 15(3):293–300, 2019.

[2] Katrina M Longhini and Michael Glotzer. Aurora a and cortical flows promote polarization and cytokinesis by inducing asymmetric ect-2 accumulation. *Elife*, 11:e83992, 2022.

[3] Mirjam Mayer, Martin Depken, Justin S Bois, Frank Jülicher, and Stephan W Grill. Anisotropies in cortical tension reveal the physical basis of polarizing cortical flows. *Nature*, 467(7315):617–621, 2010.

[4] Ani Michaud, Marcin Leda, Zachary T Swider, Songeun Kim, Jiaye He, Jennifer Landino, Jenna R Valley, Jan Huisken, Andrew B Goryachev, George von Dassow, et al. A versatile cortical pattern-forming circuit based on rho, f-actin, ect2, and rga-3/4. *Journal of Cell Biology*, 221(8):e202203017, 2022.

[5] Jonathan B Michaux, François B Robin, William M McFadden, and Edwin M Munro. Excitable rhoa dynamics drive pulsed contractions in the early c. elegans embryo. *Journal of Cell Biology*, 217(12):4230–4252, 2018.

[6] Arnab Saha, Masatoshi Nishikawa, Martin Behrndt, Carl-Philipp Heisenberg, Frank Jülicher, and Stephan W Grill. Determining physical properties of the cell cortex. *Biophysical journal*, 110(6):1421–1429, 2016.